ARTICLE - Plasma Cell Disorders

Bedaquiline amplifies proteasome inhibitor efficacy and overcomes resistance in multiple myeloma

Michela Cumerlato,[1,2] Monica Maccagno,[1,2] María Labrador,[1,2] Beatrice Luciano,[1,2] Elisabetta Mereu,[1,2] Mariangela Porro,[1,2] Cecilia Bandini,[1,2] Mattia Furlan,[3] Domenico Maisano,[4] Mattia D'Agostino,[1,5] Alessandra Larocca,[1,5] Francesca Gay,[1,5] Annalaura Tamburrini,[2,6] Francesca Anselmi,[2,6] Paolo Ettore Porporato,[1,2] Salvatore Oliviero,[2,6] Benedetto Bruno,[1,5] Eugenio Morelli,[3,7] Nikhil Munshi[4] and Roberto Piva[1,2,5]

[1]Department of Molecular Biotechnology and Health Sciences, University of Turin, Turin, Italy; [2]Molecular Biotechnology Center (MBC) "Guido Tarone", Turin, Italy; [3]Candiolo Cancer Institute, FPO-IRCCS, Turin, Italy; [4]Dana Farber Cancer Institute, Boston, MA, USA; [5]Città della Salute e della Scienza Hospital, Turin, Italy; [6]Department of Life Sciences and Systems Biology, University of Turin, Turin, Italy and [7]Department of Oncology, University of Turin, Turin, Italy

Correspondence: R. Piva
roberto.piva@unito.it

Received: November 5, 2025.
Accepted: April 16, 2026.
Early view: April 23, 2026.

https://doi.org/10.3324/haematol.2025.300157

©2026 Ferrata Storti Foundation
Published under a CC BY-NC license

SUPPLEMENTAL MATERIAL

Bedaquiline amplifies proteasome inhibitor efficacy and overcomes resistance in multiple myeloma

Michela Cumerlato[1,2], Monica Maccagno[1,2], María Labrador[1,2], Beatrice Luciano[1,2], Elisabetta Mereu[1,2], Mariangela Porro[1,2], Cecilia Bandini[1,2], Mattia Furlan[3], Domenico Maisano[4], Mattia D'Agostino[1,5], Alessandra Larocca[1,5], Francesca Gay[1,5], Annalaura Tamburrini[2,6], Francesca Anselmi[2,6], Paolo Ettore Porporato[1,2], Salvatore Oliviero[2,6], Benedetto Bruno[1,5], Eugenio Morelli[3,7], Nikhil Munshi[4], Roberto Piva[1,2,5]

[1]Department of Molecular Biotechnology and Health Sciences, University of Turin, Turin, Italy;
[2]Molecular Biotechnology Center (MBC) "Guido Tarone", Turin, Italy;
[3]Candiolo Cancer Institute, FPO-IRCCS, Turin, Italy;
[4]Dana Farber Cancer Institute, Boston, MA, United States;
[5]Città della Salute e della Scienza Hospital, Turin, Italy;
[6]Department of Life Sciences and Systems Biology, University of Turin, Turin, Italy; [7]Department of Oncology, University of Turin, Turin, Italy.

CONTENTS

Supplementary Materials and Methods 3

- Cell Culture Conditions and Reagents
- Synergy Score
- Virus Production and In Vitro Transduction
- Gene Silencing and Overexpression of ATP5F1C
- Ub-G76V-GFP Proteasome Inhibition Reporter
- ATP-Lite Assay
- CCK-8 Assay
- Cell Cycle and Cell Viability Assays
- Proteasome Activity Assay
- Mitochondrial Superoxide Detection
- Measurement of Oxygen Consumption Rate
- Immunoblotting
- RNA Extraction and RT-qPCR
- RNA-Sequencing
- Prognostic Analysis in the CoMMpass Dataset
- Mass Spectrometry and Proteomic Data Analysis
- 2D Co-culture
- 3D Co-culture
- Statistical Analyses

Supplementary References 10

Supplementary Figures and Legends 11

- Supplementary Figure 1. Synergistic effects of BDQ and BDQ-F with CFZ across MM cell lines
- Supplementary Figure 2. ATP5F1C knockdown and overexpression efficiency; BDQ–CFZ effects on oxygen consumption rate and mitochondrial ROS levels
- Supplementary Figure 3. Modulation of apoptosis, DNA damage, survival-, and cell-cycle–associated proteins following BDQ and CFZ treatment
- Supplementary Figure 4. RNA-sequencing time course and gene expression validation following BDQ–CFZ treatment
- Supplementary Figure 5. Overview GSEA analysis in AMO-1 cells treated with BDQ, CFZ, or BDQ–CFZ

- Supplementary Figure 6. Representative GSEA enrichment plots in AMO-1 cells
- Supplementary Figure 7. Integrated RNA-seq and proteomics heatmaps highlighting cellular stress–associated gene and protein modulation following BDQ–CFZ treatment
- Supplementary Figure 8. Selective enhancement of chymotrypsin-like proteasome activity by BDQ–CFZ
- Supplementary Figure 9. Synergistic interaction of BDQ with additional proteasome inhibitors
- Supplementary Figure 10. Lack of synergy between BDQ and non-UPS targeting agents
- Supplementary Figure 11. Assessment of stromal and total cell viability in co-culture models following BDQ–CFZ treatment
- Supplementary Figure 12. Independent prognostic impact of ATP5F1C expression in the CoMMpass cohort

Supplementary Tables (provided in a separate Excel file)

- Supplementary Table S1. Top 14 compounds from the secondary drug screen showing synergy with CFZ in five MM cell lines.
- Supplementary Table S2. Cytogenetic and clinical features of MM patients included in ex vivo assays.
- Supplementary Table S3. Concentrations of BDQ and CFZ used for MM cell line treatment and cell viability assay.
- Supplementary Table S4. Concentrations of BDQ and CFZ used for B-cell malignancy cell line treatments and cell viability.
- Supplementary Table S5. Concentrations of BDQ and CFZ used for the treatment of bone marrow-derived mononuclear cells (BMMCs).
- Supplementary Table S6. List of oligonucleotide sequences used in this study.
- Supplementary Table S7. Primary antibodies employed in this study.

SUPPLEMENTARY MATERIALS AND METHODS

Cell Culture Conditions and Reagents

Human multiple myeloma (MM) cell lines, KMM-1, U-266, KMM-1^{PIR}, U-266^{PIR}, KMS-11, NCI-H929, LP-1, AMO-1, OPM-2, KMS-18, KMS-26, KMS-28, KMS-34, RPMI-8226, SK-MM-1, MOLP-8, and JJN-3, along with the murine MM cell line 5TGM1, the chronic myelogenous leukemia cell line K-562, the human stromal cell line HS-5, the Burkitt lymphoma (BL) cell lines (RAJI, HS-Sultan, Daudi, BL-41, and Namalwa), the mantle cell lymphoma (MCL) cell lines (Granta-519 and Mino), and the diffuse large B-cell lymphoma (DLBCL) cell lines including RIVA and U-2932 (ABC-DLBCL), and OCI-LY8, SU-DHL-6, SU-DHL-7, DoHH2, and KARPAS-422 (GCB-DLBCL) were obtained from the DSMZ (Braunschweig, Germany), the ATCC (Manassas, VA, USA), or generated in-house. All cell lines were authenticated by DNA fingerprinting using the GenePrint system (Promega, Madison, WI, USA). Drug-resistant MM lines AMO-1^{CFZ-R}, AMO-1^{BTZ-R}, RPMI-8226^{CFZ-R}, and RPMI-8226^{BTZ-R} were kindly provided by Dr. Lenka Besse (St. Gallen, Switzerland) (1, 2). EBV-immortalized B-lymphocytes (IST-EBV-TW6B) were generously provided by Prof. Valentina Cauda (Politecnico di Torino, Italy). HS-5 (GFP+) cells and RPMI-8226 (tRFP+)-positive cells were derived by transduction with pLKO-GFP and pLemir control vectors, respectively. All cell lines, unless otherwise specified, were cultured in RPMI 1640 (EuroClone, Pero, Italy) supplemented with 10% fetal bovine serum (FBS; Sigma-Aldrich, St. Louis, MO, USA), 2 mM L-glutamine, 100 U/mL penicillin, and 100 µg/mL streptomycin (Gibco). IST-EBV-TW6B cells were maintained in RPMI 1640 with 20% FBS and 1% non-essential amino acids. HEK 293T cells (DSMZ) were cultured in DMEM with 10% FBS and the same supplementation. The AL amyloidosis cell lines ALMC-1 and ALMC-2 were maintained in Iscove's Modified Dulbecco's Medium (Gibco, Thermo Fisher Scientific) supplemented with 10% FBS (Biological Industries), 2 mM L-glutamine, 1% penicillin-streptomycin, 1 ng/mL human interleukin-6 (PeproTech), and 10 ng/ml IGF1. All cultures were maintained at 37°C in a humidified incubator with 5% CO_2. Carfilzomib (CFZ), bortezomib (BTZ), ixazomib (IXA), melphalan (MEL), doxorubicin (DOX), dexamethasone (DEXA), lenalidomide (LENA), venetoclax (VEN), bedaquiline (BDQ), BDQ-fumarate (BDQ-F), and ATP synthase inhibitor 1 (ATPSi) were purchased from Selleckchem (Munich, Germany) or MedChemExpress (Stockholm, Sweden). TAK-243 (TAK) was obtained from TargetMol (Boston, MA, USA).

Synergy Score

Synergistic score of the combinatorial treatment with BDQ or BDQ-F and CFZ was assessed using SynergyFinder+. The score was calculated based on either the Bliss Score (BS) or the ZIP Score.

Virus Production and In Vitro Transduction

High-titer lentiviral stocks were generated in 293T cells by co-transfecting the expression vector (pLKO, pLX304, or pLX301) with packaging vectors (pCMVdR8.74 and VSV-G/pMD2.G), using the Effectene Transfection Reagent (Qiagen, Milan, Italy) according to the manufacturer's protocol. Viral supernatants were collected over 36–60 hours, filtered through a 0.22 µm filter, and concentrated using the Lenti-X Concentrator (ClonTech). Concentrated viruses were resuspended in cold phosphate-buffered saline (PBS) and stored at –80°C. Cells (1 × 10^5/mL) were transduced in the presence of 8 µg/mL polybrene. Fresh medium was added 2 hours post-infection. Stable cell lines were selected using 1 µg/mL puromycin or blasticidin (Sigma-Aldrich). Cell viability was assessed at 48 or 72 hours post-transduction (hpt) using tetramethylrhodamine methyl ester (TMRM; Molecular Probes, Eugene, OR, USA) and flow cytometry.

Gene Silencing and Overexpression of ATP5F1C

Lentiviral vectors encoding short hairpin RNAs (shRNAs) targeting ATP5F1C (shATP5F1C) or a non-targeting control (shCTRL) were generated by subcloning the respective sequences into the pLKO.1-puro vector (Addgene #8453) using AgeI–EcoRI restriction sites. shRNA sequences are listed in Supplementary Table S6. AMO-1 cells were transduced with shATP5F1C or shCTRL lentiviruses, selected with puromycin, and silencing efficiency was confirmed by RT-qPCR and immunoblotting.

For overexpression, the ATP5F1C open reading frame was obtained from the DNASU plasmid repository (pLX304-ATP5F1C, HsCD00441174) and used to produce lentiviruses. AMO-1 cells were transduced with pLX304-ATP5F1C or empty vector (pLX304), followed by blasticidin selection. Overexpression was validated by RT-qPCR and immunoblotting.

Ub-G76V-GFP Proteasome Inhibition Reporter

The pLX301_Ub-G76V-GFP vector was derived from pEGFP-N1-Ub-G76V-GFP (Addgene #11941, gift from Nico Dantuma). For proteasome inhibition assays, MM cell lines AMO-1_UbGFP and AMO-1_UbGFP$^{BTZ\text{-}R}$ were seeded at 1x10^5 cells/mL. AMO-1_UbGFP and AMO-1_UbGFP$^{BTZ\text{-}R}$ cells were treated with 2.5 nM and 12.5 nM CFZ, respectively, 10 µM BDQ, or their combination. Cell viability was assessed by TMRM staining, and GFP-positive cells along with their fluorescence intensity were analyzed by flow cytometry and

fluorescence microscopy using a ZEISS Axio Observer inverted microscope (10× objective) at 10, and 24 hpt.

ATP-Lite Assay

Cell viability/proliferation was measured using the CellTiter-Glo® Luminescent Cell Viability Assay (Promega). Cells were seeded at 1 × 10^5/mL and analyzed at day 0 and at the indicated timepoints. Ten microliters of cells were mixed with an equal volume of CellTiter-Glo® reagent in a white 384-well plate, in technical duplicate. Plates were shaken in the dark for 2 minutes and incubated at room temperature (RT) for 10 minutes. Luminescence was measured using the Synergy™ 2 Multi-Mode Microplate Reader (BioTek Instruments, Winooski, VT, USA).

CCK-8 Assay

Cell viability/proliferation was also assessed using the Cell Counting Kit-8 (CCK-8; Dojindo). Cells were plated at 1 × 10^5/mL and evaluated at day 3 or day 4. 90 µL of cell suspension were mixed with 10 µL of CCK-8 reagent in a 96-well plate, in technical quadruplicate. Plates were incubated at 37°C for 1–4 hours (without CO_2). Absorbance at 450 nm was measured using the Synergy™ 2 reader.

Cell Cycle and Cell Viability Assays by Flow Cytometry

Apoptosis was measured by flow cytometry after staining with tetrametylrodamine methyl ester (TMRM; Molecular Probes, Eugene, Oregon, USA) or Annexin V-FITC Kit (Miltenyi Biotec, Bergisch Gladbach, Germany), according to the manufacturer's instructions. $CD138^+$ cells were identified using anti-human CD138-APC (clone 44F9; Miltenyi). Cell cycle analysis was performed by PI staining. Cells were washed in PBS, incubated with RNase (0.14 mg/mL) and stained with PI (28.57 µg/mL). Data were acquired using BD FACSCelesta™ or BD Accuri™ instruments and analyzed with FACSDiva v8.0 (BD Biosciences).

Proteasome Activity Assay

Chymotrypsin-like, trypsin-like, and caspase-like proteasome activities were measured using the Proteasome-Glo™ Cell-Based Assay (Promega, G1180) according to the manufacturer's protocol. MM cell lines AMO-1, KMS-11, RPMI-8226, MOLP-8, U-266 cell lines were plated at 1×10^5 cells/mL and treated with 2.5 nM CFZ, 5 µM BDQ, or their combination. Proteasome activity was assessed 5 hours post-treatment in technical quadruplicates. For each condition, 50 µL of cell suspension was combined with 50 µL of the appropriate Proteasome-Glo™ reagent (Chymotrypsin-like, Trypsin-like, or Caspase-like) in white 96-well plates. Plates were shaken at 700 rpm for 2 minutes and incubated for

10 minutes at room temperature in the dark. Luminescence was recorded using a Synergy™ 2 Multi-Mode Microplate Reader (BioTek Instruments, Winooski, VT).

Mitochondrial Superoxide Detection

Mitochondrial superoxide was measured using the MitoSOX™ Red Indicator (Thermo Fisher Scientific), according to the manufacturer's protocol, and analyzed by flow cytometry.

Measurement of Oxygen Consumption Rate

Oxygen consumption rate (OCR) was monitored over time using the Resipher™ system (Lucid Scientific, Atlanta, GA, USA). AMO-1 cells were seeded at 20,000 cells/well in 96-well plates and incubated at 37 °C, 5% CO_2. OCR was recorded via the Lucid Lab web app, with data captured every 60 minutes, and monitored for 36 h after treatment with CFZ and BDQ at the indicated concentrations. Measurements are the average of five independent replicates.

immunoBlotting

Cells were lysed in buffer (20 mM Tris-HCl pH 7.4, 150 mM NaCl, 5 mM EDTA, 1% Triton X-100, 1 mM PMSF, 10 mM NaF, 1 mM Na_3VO_4, and protease inhibitors; Roche). Lysates were incubated at 4°C for 30 min, centrifuged at 13,000 × g for 15 min, and protein quantified by Bio-Rad DC assay. Equal amounts of protein were resolved by SDS-PAGE, transferred to nitrocellulose membranes, blocked in 5% milk in PBS-T for 1 h, then incubated overnight with primary antibodies in 5% BSA + NaN_3. Membranes were washed and incubated with secondary antibodies for 1 h, then visualized with Immobilon immunoHRP substrate (Merck). Antibodies used are listed in Supplementary Table S7.

RNA Extraction and Reverse Transcription-quantitative PCR (RT-qPCR)

Total RNA was isolated using the RNeasy Mini Kit (Qiagen). RNA was treated with RQ1 RNase-free DNase (Promega) and reverse-transcribed using the OneScript Plus cDNA Synthesis Kit (ABM, Canada) or SuperScript III (Invitrogen, Carlsbad, CA, USA). RT-qPCR was performed in 384-well plates on a Bio-Rad iCycler using iQ SYBR Green or BlasTaq™ 2X qPCR MasterMix (ABM), following manufacturer instructions. Cycling: 95°C for 10 min, then 40 cycles of 95°C for 15 s and 60°C for 1 min. Primer sequences (designed via PrimerBLAST) are listed in Supplementary Table S6. Specificity was validated by melting curve, standard curve slope, and linearity. GAPDH served as the endogenous control. Expression levels were normalized to control infections (scrambled shRNA, empty vector, or uninfected).

RNA-sequencing

AMO-1 cells were treated with DMSO, CFZ (2.5 nM), BDQ (5 μM), or their combination, and harvested at 6, 12, and 18 hpt. RNA was extracted using the RNeasy Mini Kit and quality assessed via Agilent TapeStation. Libraries were prepared with the TruSeq Stranded mRNA Kit (Illumina) and sequenced on the Illumina NextSeq 1000. Reads were aligned to hg38 using STAR v2.7.1a. Gene counts were obtained with featureCounts v1.6.3 using GENCODE v42 (3). Differential expression was determined by GLM and likelihood ratio tests; genes with |logFC| >1 and FDR <0.01 were considered significant. Gene set enrichment was performed using the SnakeGSEA pipeline with multiGSEA (https://github.com/molinerisLab/SnakeGSEA) (4). Genes were ranked according to the signed statistic derived from the differential expression analysis for each contrast (BDQ vs Ctrl, CFZ vs Ctrl, BDQ-CFZ vs Ctrl). Enrichment was evaluated using gene sets from the Hallmark (MSigDB), KEGG, and Gene Ontology (GO) collections. Default parameters were applied, and statistical significance was assessed based on normalized enrichment scores (NES) and false discovery rate (FDR q-value). Representative enrichment plots were generated for selected pathways of interest. Heatmaps were generated using the ComplexHeatmap R package (5).

Prognostic analysis in the CoMMpass dataset

Gene expression and clinical data were retrieved from the CoMMpass study (IA21 release). Expression levels of ATP5F1A, ATP5F1B, and ATP5F1C (Salmon unstranded TPMs) were obtained together with overall survival (OS) and progression-free survival (PFS) data and corresponding censoring indicators. Patients were stratified according to gene expression levels using the top 30% of each gene expression distribution as the high-expression group. Kaplan–Meier survival curves were generated for OS and PFS, and group differences were assessed using the log-rank test with correction for multiple testing.

To evaluate the independent prognostic value of ATP5F1C, multivariable Cox proportional hazards regression models were fitted including: ATP5F1C expression (top 30% vs remaining patients), age (continuous variable), CGS high-risk classification (binary variable) developed by the International Myeloma Society and the International Myeloma Working Group (6). This classification integrates recurrent cytogenetic alterations and serum biomarkers. CGS status was reconstructed in the CoMMpass dataset using copy number estimates, somatic mutation calls, Seq-FISH data, and baseline clinical measurements. Gene-level copy number values were used as proxies for chromosomal alterations (e.g., CDKN2C for del(1p32), TP53 for del(17p13), and CKS1B for 1q gain). Log_2 ratio thresholds

were applied to define gains and monoallelic or biallelic deletions, consistent with the original publication. Baseline serum biomarker measurements were used for risk classification.

All survival analyses were restricted to 631 patients with complete CGS component data and available ATP5F1 expression levels in CD138-positive bone marrow plasma cells at baseline. The proportional hazards assumption was evaluated using Schoenfeld residuals, and no violations were detected (all p-values > 0.05). Data manipulation, statistical analyses, and visualization were performed in R using the readr, survival, and survminer packages. The R script used for these analyses is available upon request.

Mass Spectrometry (MS) and Proteomic Data Analysis

Cells were lysed by boiling at 95°C for 10 minutes in 100 mM triethylammonium bicarbonate (TEAB) containing 2% sodium deoxycholate (SDC), 40 mM chloroacetamide, and 10 mM tris(2-carboxyethyl)phosphine (TCEP), followed by sonication (Bandelin Sonoplus Mini 20, MS 1.5). Protein concentration was determined using the BCA Protein Assay Kit (Thermo Scientific), and 30 µg of protein per sample was used for MS preparation. The volume was adjusted to 50 µL with 100 mM TEAB containing 2% SDC. Samples were processed using the SP3 protocol, as described by Hughes et al. Briefly, 5 µL of SP3 beads were added to 30 µg of protein, and the final volume was brought to 50 µL with 100 mM TEAB. Ethanol was added to a final concentration of 60% (v/v) to induce protein binding. Samples were mixed and incubated for 5 minutes at room temperature (RT). After magnetic separation, the supernatant was discarded, and the beads were washed twice with 180 µL of 80% ethanol. Proteins were digested on-bead overnight at 37°C using trypsin at a 1:30 enzyme-to-protein ratio, in 100 mM TEAB. Following digestion, samples were acidified to 1% trifluoroacetic acid (TFA) and desalted using in-house packed C18 stage tips (Empore disks (7). Peptides were analyzed by nanoLC-MS/MS using an Aurora Ultimate TS column (25 cm × 75 µm ID, 1.7 µm particles; Ion Opticks). Mobile phase A consisted of water with 0.1% formic acid, and mobile phase B consisted of acetonitrile with 0.1% formic acid. Samples were first loaded onto a trap column (C18 PepMap100, 5 µm, 300 µm × 5 mm; Thermo Scientific) for 4 minutes at 18 µL/min using a loading buffer of water, 2% acetonitrile, and 0.1% TFA. Peptides were then eluted with a linear gradient from 4% to 35% B over 60 minutes. Eluted peptides were ionized by electrospray and analyzed on a Thermo Scientific Orbitrap Ascend in data-independent acquisition (DIA) mode. Survey scans were acquired from 350–1400 m/z at 60,000 resolution (at 200 m/z) with an ion target of 4×10^5. DIA scans were collected at 30,000 resolution with an AGC target of 1000% and maximum injection time set to "Auto." The 400–1000 m/z range was segmented into 30 windows of 20 Da each.

HCD fragmentation was performed at a normalized collision energy of 28%. Data were processed and quantified using Spectronaut 18 in directDIA mode (8). Searches were conducted against the human UniProt database (June 2023 release; 20,605 entries). Enzyme specificity was set to C-terminal cleavage after Arg and Lys, allowing cleavage at proline residues and up to two missed cleavages. Carbamidomethylation of cysteines was defined as a fixed modification; N-terminal acetylation and methionine oxidation were set as variable modifications. False discovery rate (FDR) was controlled at 1% for peptide-spectrum matches (PSMs), peptides, and proteins. Quantification was based on MS2-level data. Precursor and protein posterior error probability (PEP) thresholds were set to 0.01 and 0.05, respectively. Processed data were exported and further analyzed using Perseus v1.6.15.0 (9).

2D Co-culture

HS-5 (GFP^+) and AMO-1 cells were seeded in 24-well plates at 5×10^4/mL and 1×10^5/mL, respectively. Cells were treated with CFZ (2.5 nM), BDQ (5 μM), or the combination at day 0 and 3. Every 3 days, cells were collected and replated. Cell viability was assessed by flow cytometry using propidium iodide exclusion prior to lineage marker analysis.

3D Co-culture

3D scaffolds were prepared following the protocol by Belloni et al. (10) with adaptations for multiple myeloma (MM) cell culture under static conditions. Briefly, scaffold discs were created from Spongostan™ sheets (Ethicon, Inc., Somerville, NJ, USA) using a sterile 4 mm biopsy punch. Each disc was pre-seeded with $2x10^5$ GFP-positive HS-5 stromal cells. After 24 hours, $5x10^5$ tRFP-positive SK-MM-1 cells were added to each scaffold. The scaffolds were then cultured in 1 mL of RPMI-1640 medium in 24-well plates. To minimize the presence of non-adherent cells, the scaffolds were transferred to new wells every 24 hours for three days. Drug treatments were administered 72 hours after seeding the SK-MM-1 cells, using sublethal doses of CFZ, BDQ, or a combination of the two drugs. Six days post-treatment, cells were released from the scaffolds using Liberase™ (25 μg/mL, Merck Millipore, Burlington, MA, USA) and analyzed by flow cytometry to assess the ratio of stromal and tumor cells.

Statistical analyses

Statistical analyses were performed with GraphPad Prism 10 (GraphPad Software Inc.). Statistical significance of differences observed (in both *in vitro* and *in vivo* experiments) was determined by Student t test or one-way ANOVA; differences were considered significant when P value was <.05 (*), <.01 (**), <.001 (***), or <.0001 (****)

SUPPLEMENTAL REFERENCES

1. Besse L, Besse A, Mendez-Lopez M, et al. A metabolic switch in proteasome inhibitor-resistant multiple myeloma ensures higher mitochondrial metabolism, protein folding and sphingomyelin synthesis. Haematologica. 2019; 104(9):e415-e419.
2. Soriano GP, Besse L, Li N, et al. Proteasome inhibitor-adapted myeloma cells are largely independent from proteasome activity and show complex proteomic changes, in particular in redox and energy metabolism. Leukemia. 2016; 30(11):2198-2207.
3. Liao Y, Smyth GK, Shi W. featureCounts: an efficient general purpose program for assigning sequence reads to genomic features. Bioinformatics. 2014; 30(7):923-30.
4. Canzler S, Hackermuller J. multiGSEA: a GSEA-based pathway enrichment analysis for multi-omics data. BMC Bioinformatics. 2020; 21(1):561.
5. Gu Z, Eils R, Schlesner M. Complex heatmaps reveal patterns and correlations in multidimensional genomic data. Bioinformatics. 2016; 32(18):2847-9.
6. Avet-Loiseau H, Davies FE, Samur MK, et al. International Myeloma Society/International Myeloma Working Group Consensus Recommendations on the Definition of High-Risk Multiple Myeloma. J Clin Oncol. 2025; 43(24):2739-2751.
7. Rappsilber J, Mann M, Ishihama Y. Protocol for micro-purification, enrichment, pre-fractionation and storage of peptides for proteomics using StageTips. Nat Protoc. 2007; 2(8):1896-906.
8. Bruderer R, Bernhardt OM, Gandhi T, et al. Extending the limits of quantitative proteome profiling with data-independent acquisition and application to acetaminophen-treated three-dimensional liver microtissues. Mol Cell Proteomics. 2015; 14(5):1400-10.
9. Tyanova S, Temu T, Sinitcyn P, et al. The Perseus computational platform for comprehensive analysis of (prote)omics data. Nat Methods. 2016; 13(9):731-40.
10. Belloni D, Ferrarini M, Ferrero E, et al. Protocol for generation of 3D bone marrow surrogate microenvironments in a rotary cell culture system. STAR Protoc. 2022; 3(3):101601.

SUPPLEMENTAL FIGURES AND LEGENDS

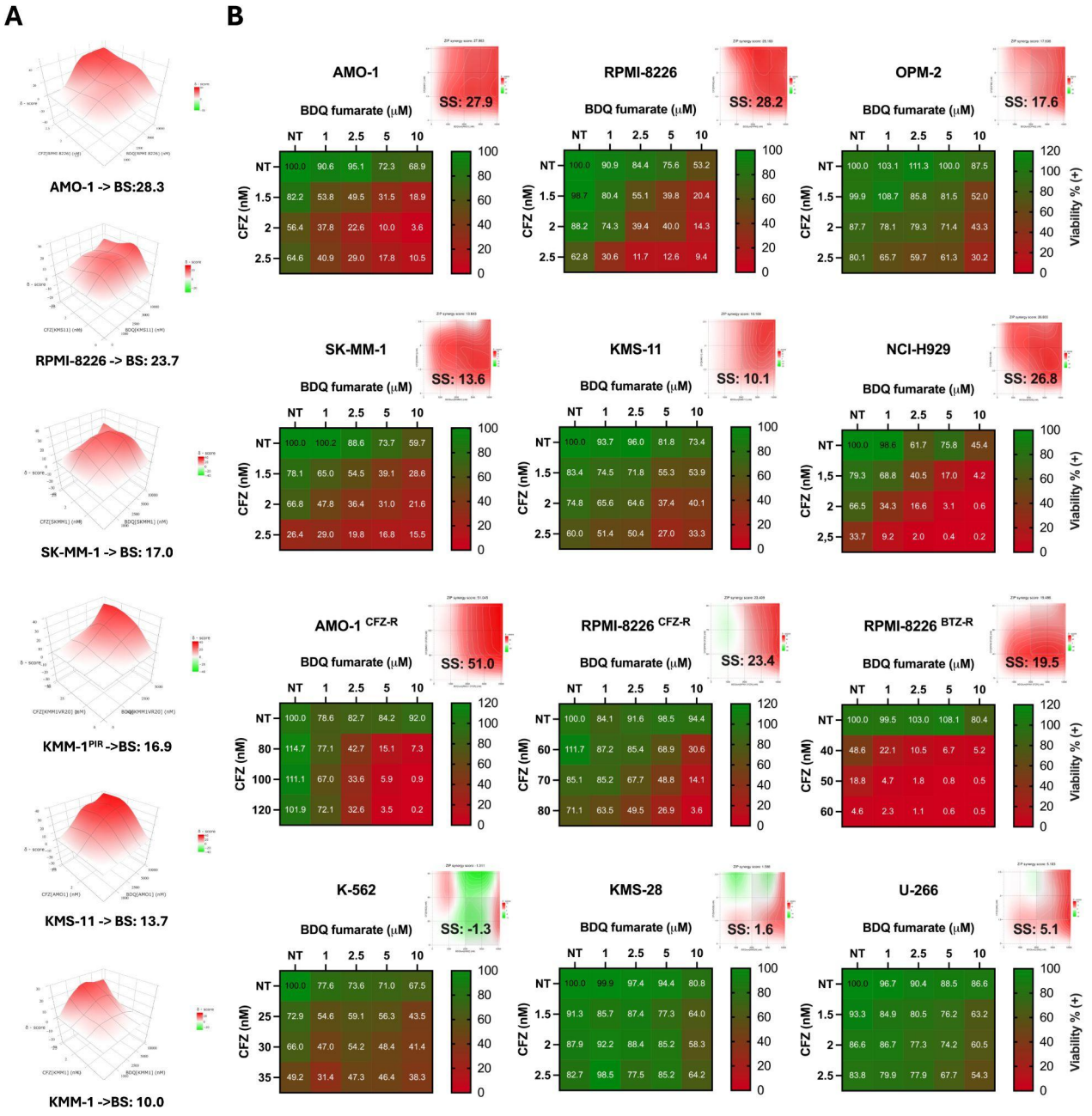

Supplementary Figure 1. Synergistic Effects of Bedaquiline (BDQ) and Its Fumarate Salt (BDQ-F) with Carfilzomib (CFZ) in Multiple Myeloma Cell Lines. (A) 3D dose-response matrices showing the combinatorial effects of BDQ and CFZ in AMO-1, RPMI-8226, KMS-11, SK-MM-1, KMM-1, and KMM-1^{PIR} cell lines. Cell viability was assessed by TMRM staining and analyzed by flow cytometry 72 hours post-treatment. Bliss synergy (BS) scores were calculated using the SynergyFinder+ tool (www.synergyfinder.org). **(B)** Dose-response matrices of BDQ-F and CFZ combinations across a panel of MM cell lines and the K-562 chronic myeloid leukemia cell line. Viability was measured using CellTiter-Glo® Luminescent assay 72 hours post-treatment and normalized to luminescence values at time 0. Synergy scores (SS) were calculated using the Bliss independence model.

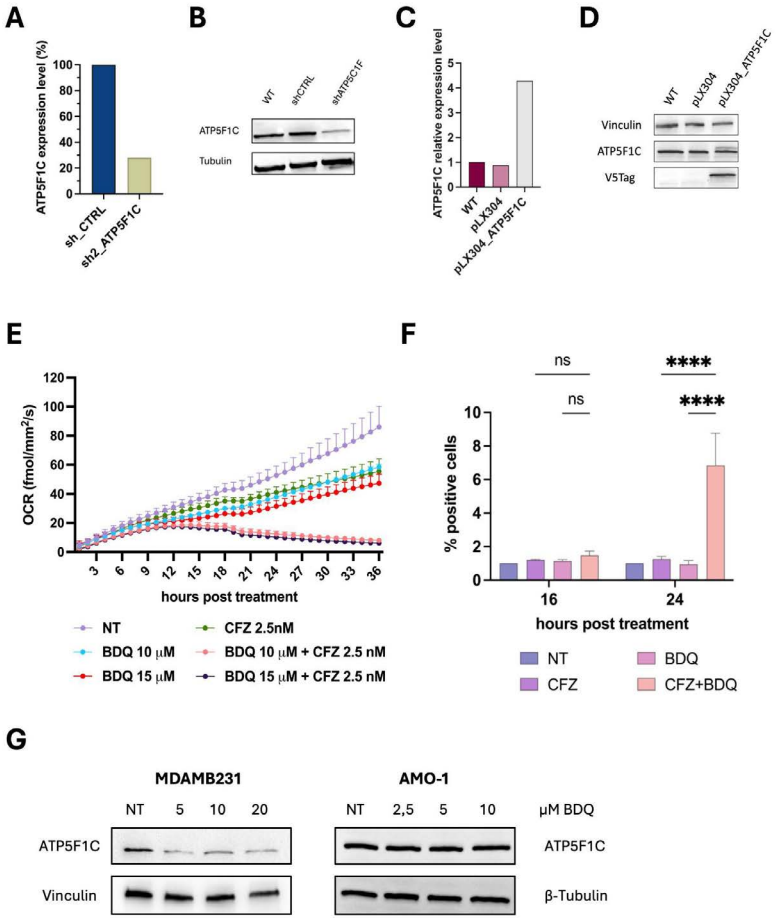

Supplementary Figure 2. ATP5F1C Knockdown and Overexpression Efficiency; BDQ-CFZ Effects on Oxygen Consumption Rate and Mitochondrial ROS Levels. (A) ATP5F1C knockdown efficiency in AMO-1 cells transduced with shRNA targeting ATP5F1C (sh2_ATP5F1C) or scrambled control (shCTRL), quantified by RT-qPCR following puromycin selection. ATP5F1C expression levels were normalized to a housekeeping gene and are shown as relative expression values. Data represent mean ± SD of three independent biological replicates (n = 3). **(B)** Representative immunoblot showing ATP5F1C protein levels in AMO-1 cells expressing shCTRL or sh2_ATP5F1C. α-Tubulin was used as a loading control. **(C)** Relative ATP5F1C expression in AMO-1 cells transduced with empty vector (pLX304) or pLX304_ATP5F1C, assessed by RT-qPCR to confirm overexpression. Expression levels were normalized to a housekeeping gene and are shown as mean ± SD (n = 3). **(D)** Representative immunoblot of ATP5F1C and V5-tag in AMO-1 cells transduced with pLX304 vector or pLX304_ATP5F1C. V5-tag detection confirms ectopic ATP5F1C expression. Vinculin was used as a loading control. **(E)** BDQ–CFZ combination reduced oxygen consumption rate (OCR) compared to single treatments. OCR (fmol/min/mm²) was recorded for 36 hours using the Resipher™ system following treatment with CFZ (2.5 nM) and BDQ (10 or 15 µM) at the indicated concentrations. Data represent mean ± SD of three independent experiments (n = 3). **(F)** Mitochondrial superoxide generation in AMO-1 cells was measured by flow cytometry (MitoSOX staining) at 16 and 24 hours post-treatment with CFZ (2.5 nM), BDQ (5 µM), or the combination. Data are shown as mean ± SD of three independent experiments (n = 3). Statistical significance was determined by one-way ANOVA (****p < 0.0001; ns, not significant). **(G)** Representative immunoblot analysis of ATP5F1C protein levels in MDA-MB-231 and AMO-1 cells following 24-hour treatment with increasing concentrations of BDQ (as indicated). Vinculin (MDA-MB-231) and β-Tubulin (AMO-1) were used as loading controls.

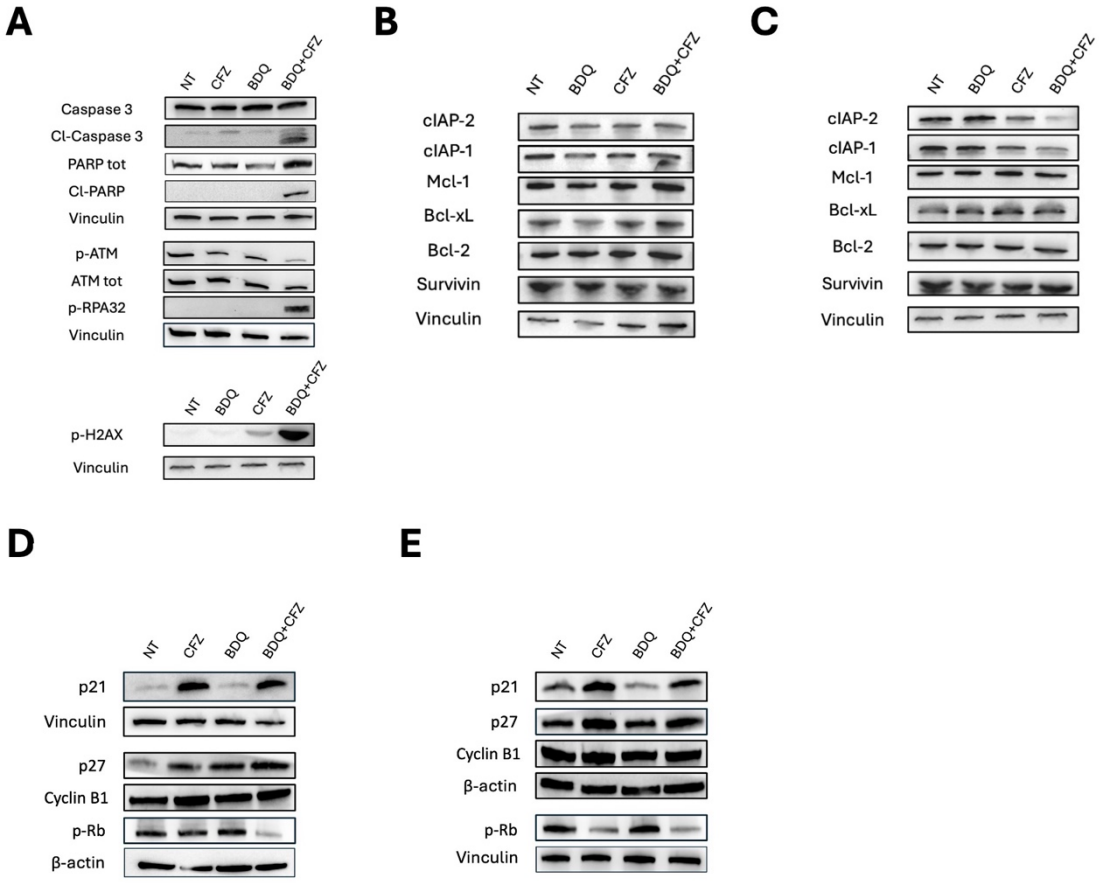

Supplementary Figure 3. Modulation of apoptosis, DNA damage, survival-, and cell-cycle–associated proteins following BDQ and CFZ treatment. (A) Representative immunoblot analysis of apoptosis- and DNA damage–associated proteins in RPMI-8226 cells treated for 16 hours with BDQ (5 μM), CFZ (2.5 nM), BDQ–CFZ, or NT. Cleaved Caspase-3, total and cleaved PARP, phospho-H2AX (γH2AX), phospho-ATM, total ATM, and phospho-RPA32 were assessed as indicated. Vinculin was used as a loading control. **(B–C)** Representative immunoblot analysis of pro-survival and anti-apoptotic proteins in AMO-1 (B) and RPMI-8226 (C) cells treated for 16 hours with BDQ (5 μM), CFZ (2.5 nM), BDQ–CFZ, or NT. Expression levels of cIAP-1, cIAP-2, Mcl-1, Bcl-xL, Bcl-2, and Survivin were evaluated as indicated. Vinculin was used as a loading control. **(D–E)** Representative immunoblot analysis of cell-cycle–associated proteins in RPMI-8226 (D) and AMO-1 (E) cells treated for 16 hours with BDQ (5 μM), CFZ (2.5 nM), BDQ–CFZ, or NT. Expression levels of p21, p27, Cyclin B1, and phospho-Rb (p-Rb) were assessed as indicated. β-actin was used as a loading control.

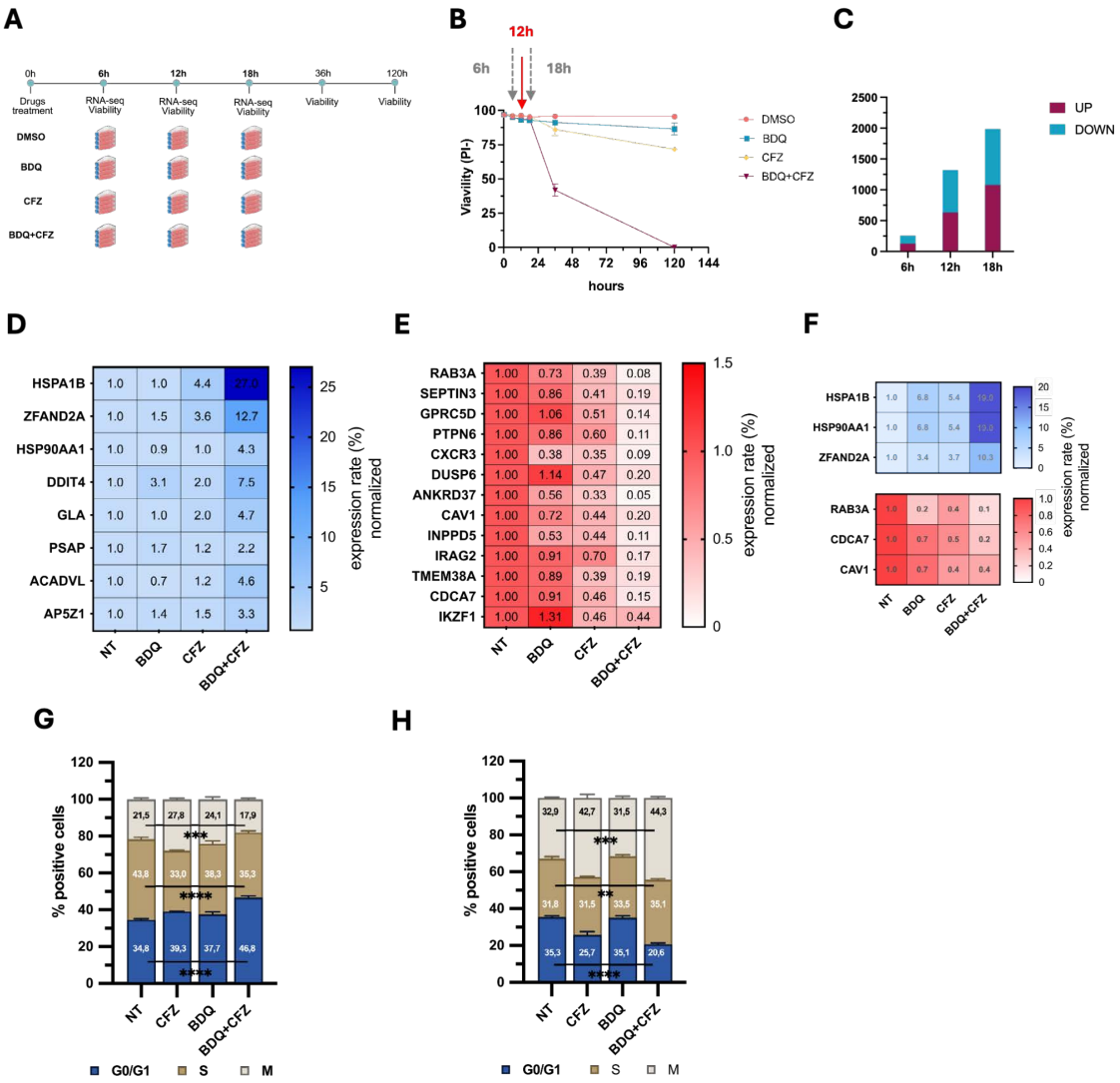

Supplementary Figure 4. RNA-sequencing time course and gene expression validation following BDQ–CFZ treatment. (A) Schematic representation of the RNA-sequencing time course. AMO-1 cells were treated with DMSO, CFZ (2.5 nM), BDQ (5 μM), or the combination (BDQ–CFZ) in biological triplicates. Cells were harvested at 6, 12, and 18 hours post-treatment for RNA-seq analysis, and cell viability was concurrently assessed at 6, 12, 18, 36, and 120 hours post-treatment. **(B)** Time-course analysis of cell viability measured by propidium iodide (PI) staining and flow cytometry. Data represent mean ± SD of three independent experiments (n = 3). **(C)** Bar graph summarizing the number of significantly upregulated (UP) and downregulated (DOWN) genes relative to DMSO at each time point. A total of 133, 637, and 1,087 genes were upregulated, whereas 124, 682, and 899 genes were downregulated at 6, 12, and 18 hours, respectively ($|\log_2 FC| > 1$, FDR <0.01). **(D–E)** Heatmaps showing RT-qPCR validation in AMO-1 cells of selected genes identified as (D) upregulated or (E) downregulated in the RNA-seq dataset following BDQ–CFZ treatment. Expression levels are shown relative to NT and normalized to a housekeeping gene. **(F)** Heatmaps showing RT-qPCR validation in RPMI-8226 cells of three upregulated and three downregulated genes following BDQ–CFZ treatment. Expression values are normalized to NT. **(G-H)** Cell cycle distribution analysis of AMO-1 (G) and RPMI-8226 (H) cells 24 hours after treatment with BDQ (5 μM), CFZ (2.5 nM), or BDQ–CFZ. Cell cycle phases (G0/G1, S, and G2/M) were determined by PI staining and flow cytometry. Data represent mean ± SD of three independent experiments (n = 3). Statistical significance was assessed by one-way ANOVA (****p < 0.0001).

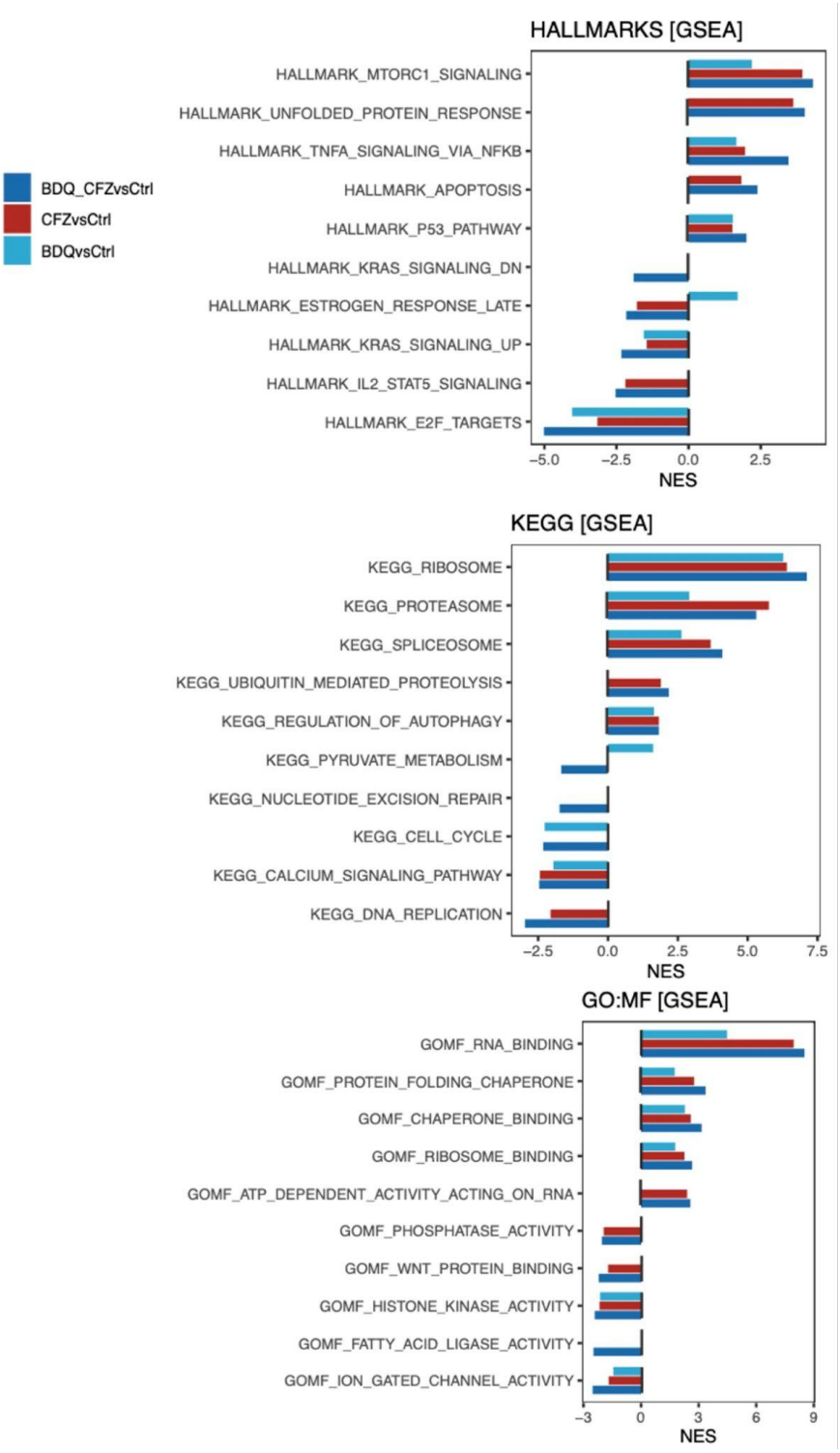

Supplementary Figure 5. GSEA overview in BDQ–CFZ–treated AMO-1 cells. Summary of gene set enrichment analysis (GSEA) from RNA-seq data in AMO-1 cells treated with BDQ, CFZ, or BDQ–CFZ. Barplots display normalized enrichment scores (NES) for selected gene sets from the Hallmark (top), KEGG (middle), and Gene Ontology Molecular Function (GO:MF; bottom) collections across the indicated contrasts. Positive NES values indicate pathway enrichment, whereas negative NES values indicate pathway suppression relative to control.

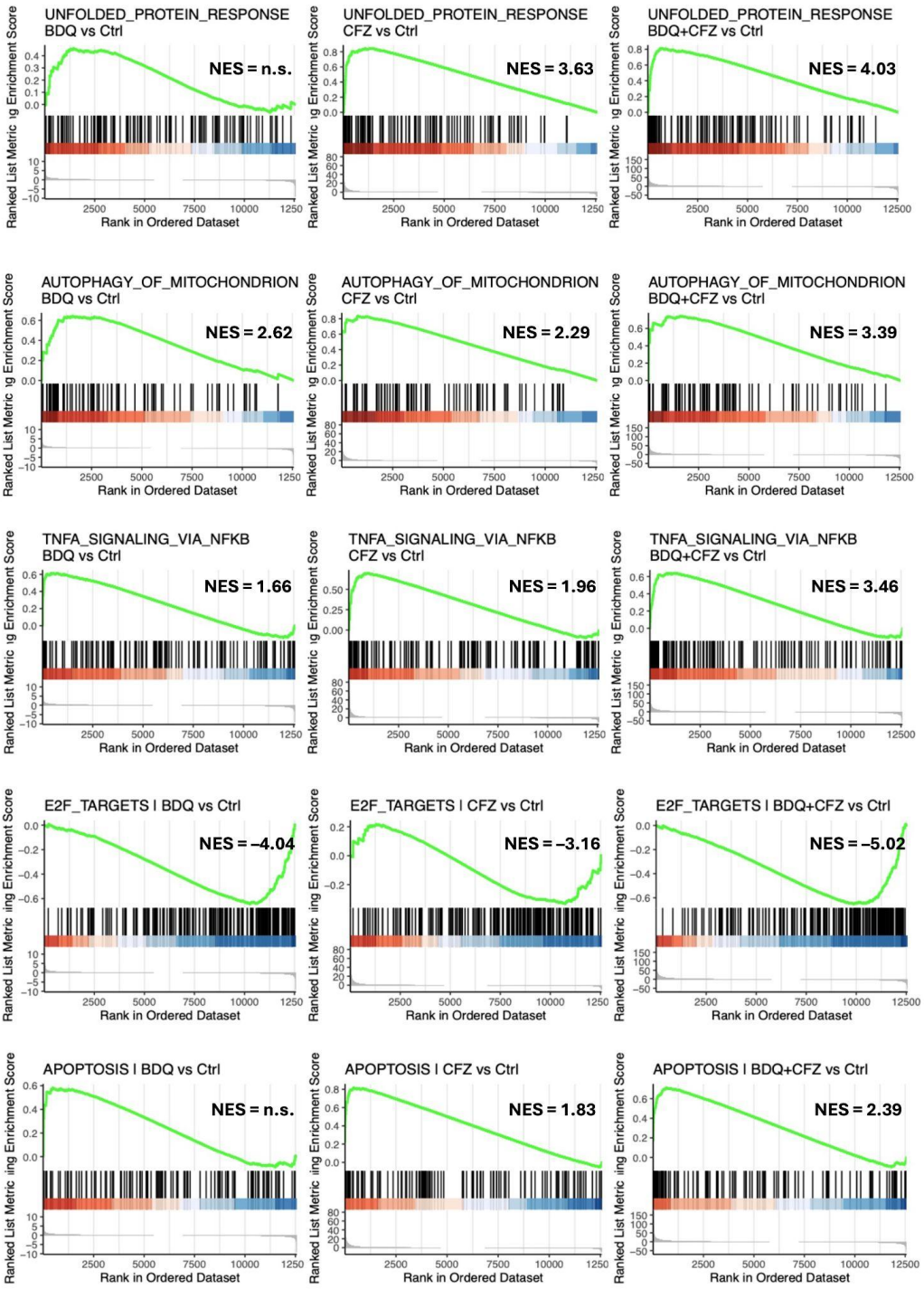

Supplementary Figure 6. Selected GSEA enrichment plots in BDQ–CFZ–treated AMO-1 cells. Representative GSEA enrichment plots from RNA-seq analysis of AMO-1 cells treated with BDQ, CFZ, or BDQ–CFZ. **(A)** Unfolded Protein Response, **(B)** Autophagy of Mitochondrion, **(C)** TNFα Signaling via NF-κB, **(D)** E2F Targets, and **(E)** Apoptosis. For each pathway, enrichment plots are shown for BDQ vs Ctrl, CFZ vs Ctrl, and BDQ–CFZ vs Ctrl, as indicated. Normalized enrichment scores (NES) are displayed within each panel. Positive NES values denote pathway enrichment, whereas negative NES values indicate pathway suppression relative to control.

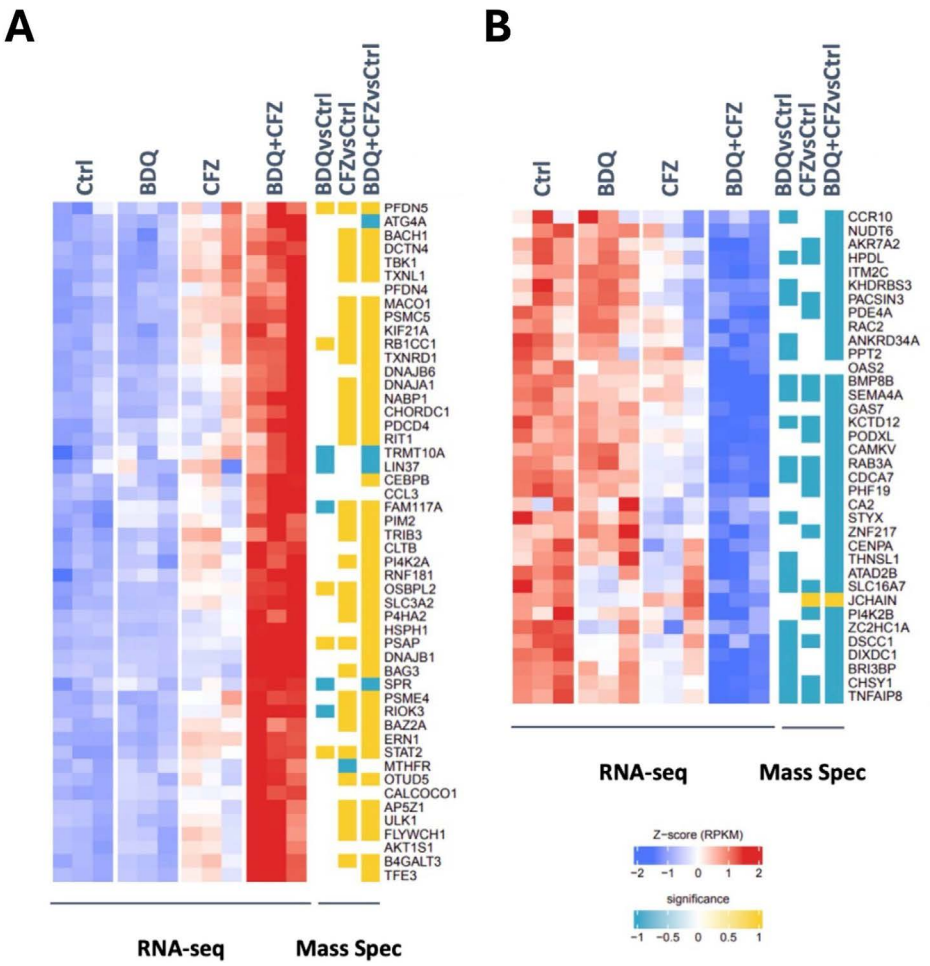

Supplementary Figure 7. Integrated RNA-seq and proteomics heatmaps highlighting cellular stress–associated gene and protein modulation following BDQ–CFZ treatment. (A) Heatmap showing transcripts and corresponding proteins significantly upregulated after BDQ–CFZ treatment, integrating RNA-seq and mass spectrometry datasets. **(B)** Heatmap showing transcripts and proteins significantly downregulated under the same conditions. Gene and protein expression levels are displayed as normalized z-scores (RNA-seq) and normalized protein expression values (mass spectrometry), as indicated by the color scale.

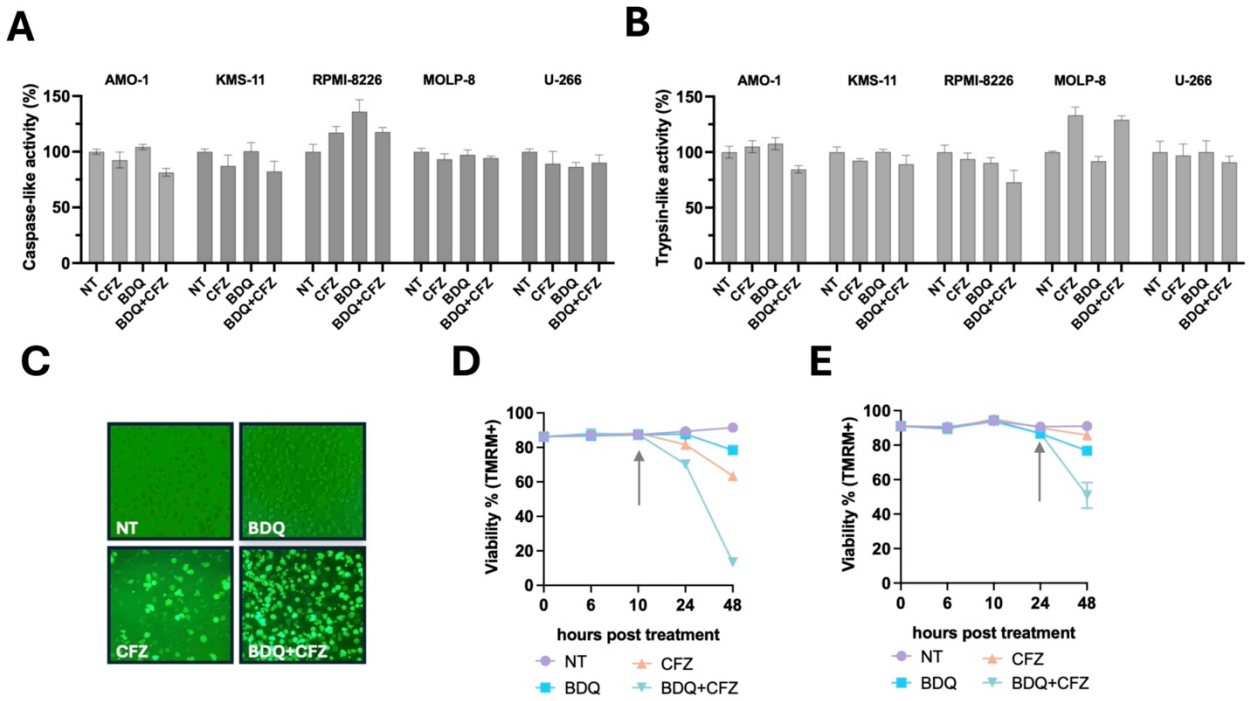

Supplementary Figure 8. BDQ Does Not Interfere with Trypsin-like and Caspase-like Proteasome Activities and Does Not Synergize with Non-proteasome-Targeting Therapies (A-B) Caspase-like **(A)** and trypsin-like **(B)** proteasome activities were measured in AMO-1, KMS-11, RPMI-8226, MOLP-8, and U-266 cell lines following 5-hour treatment with BDQ (5 μM), CFZ (2.5 nM), or their combination. **(C)** Representative fluorescence microscopy images of Ub-G76V-GFP–expressing AMO-1 cells treated with BDQ, CFZ, or the combination, showing marked GFP accumulation in BDQ-CFZ–treated cells. **(D-E)** Longitudinal cell viability analysis of Ub-G76V-GFP-expressing AMO-1 and AMO-1^{BTZ-R} cells treated with BDQ (5 μM), CFZ (2.5 nM for AMO-1 and 12.5 nM for AMO-1^{BTZ-R}), or the combination. Viability was assessed by TMRM staining and flow cytometry at multiple time points. Results represent the mean ± SD of three independent experiments.

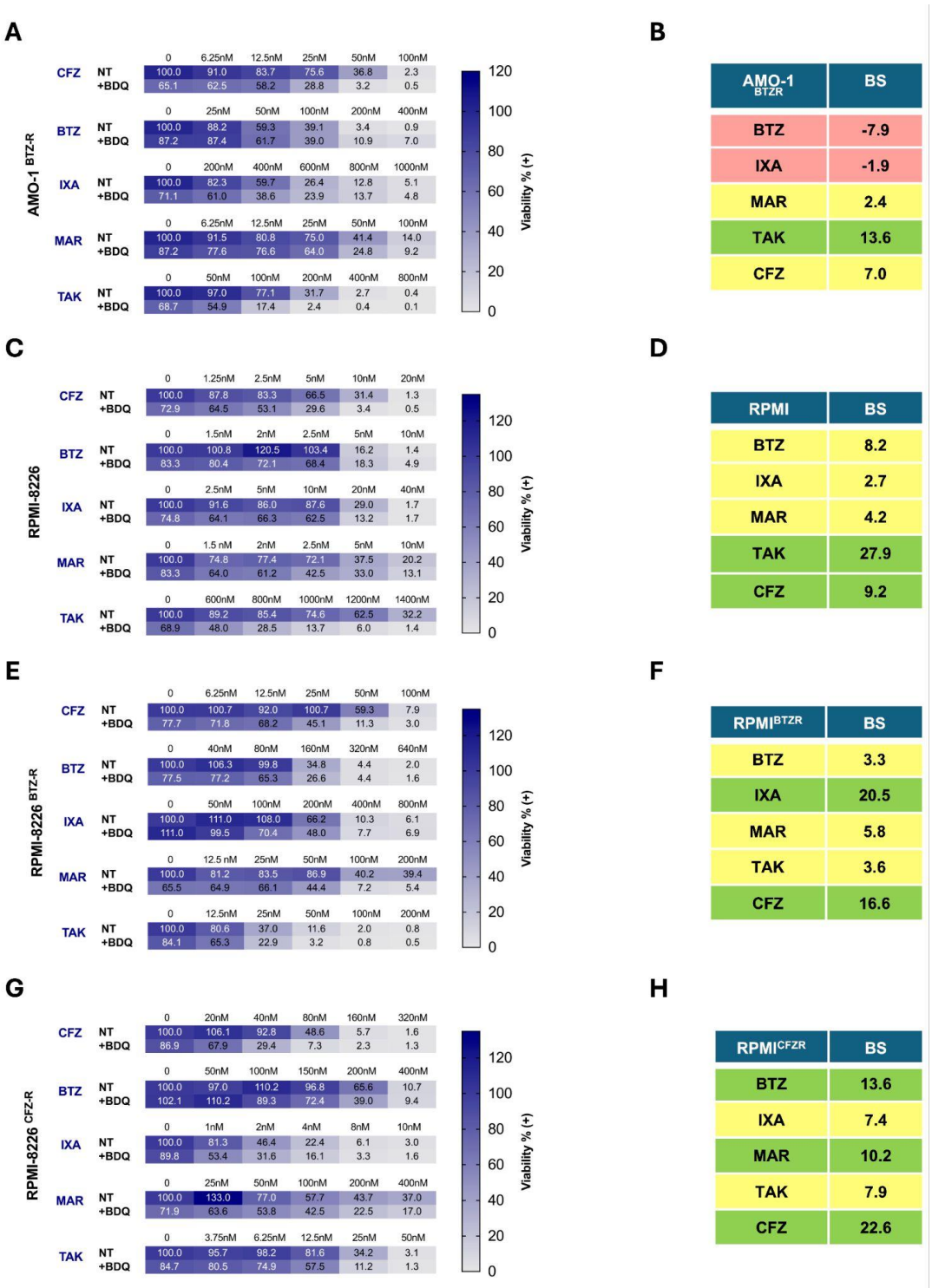

Supplementary Figure 9. BDQ Enhances the Activity of Multiple Proteasome Inhibitors in Both PI-Sensitive and -Resistant MM Cell Lines. Heatmaps of AMO-1^{BTZ-R} **(A)**, RPMI-8226 **(C)**, RPMI-8226^{BTZ-R} **(E)**, RPMI-8226^{CFZ-R} **(G)**, cell lines treated with increasing concentrations of bortezomib (BTZ), ixazomib (IXA), marizomib (MAR), TAK-243 (TAK), or carfilzomib (CFZ), with or without 10 µM BDQ. Cell viability was assessed 72 hours post-treatment by CellTiter-Glo® Luminescent. **(B, D, F, H)** Summary tables reporting the Bliss synergy scores (BS) for each drug combination across the tested cell lines. Green highlights indicate high synergistic interactions (BS > 10), yellow indicates moderate synergistic interactions (1 < BS < 10), while red indicates the absence of synergy (BS < 1).



Supplementary Figure 10. BDQ does not synergize with non-proteasome–targeting therapies. (A) Heatmap of AMO-1 cell viability following co-treatment with BDQ (5 μM) and escalating doses of Venetoclax (VEN), Melphalan (MEL), Dexamethasone (DEXA), Lenalidomide (LENA), or Doxorubicin (DOXO). Cell viability was assessed using CCK-8 assay 72 hours post-treatment.

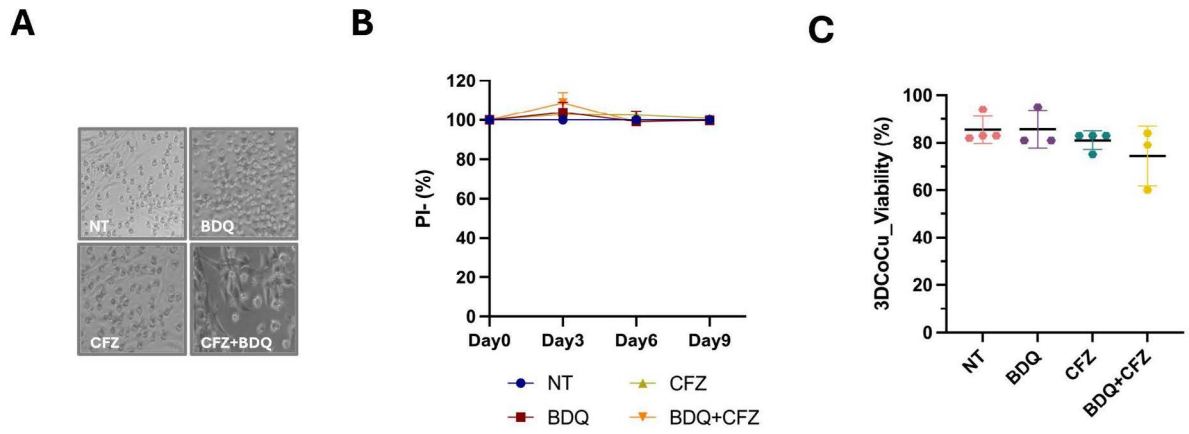

Supplementary Figure 11. Assessment of stromal and total cell viability in co-culture models following BDQ–CFZ treatment. (A) Representative bright-field images of AMO-1 cells cultured on a GFP+ HS-5 stromal monolayer and treated with DMSO (NT), BDQ (5 μM), CFZ (2.5 nM), or the combination (BDQ–CFZ). Images were acquired 3 days post-treatment. **(B)** Viability of HS-5 stromal cells in 2D co-culture following treatment with BDQ, CFZ, or BDQ–CFZ. Cell viability was assessed by propidium iodide (PI) exclusion and flow cytometry. Data represent mean ± SD of independent experiments. **(C)** Total cell viability in the 3D co-culture system (HS-5 and SK-MM1 cells) following treatment with CFZ, BDQ, or BDQ–CFZ. Viability was determined by flow cytometry 6 days post-treatment. Data represent mean ± SD of independent experiments.

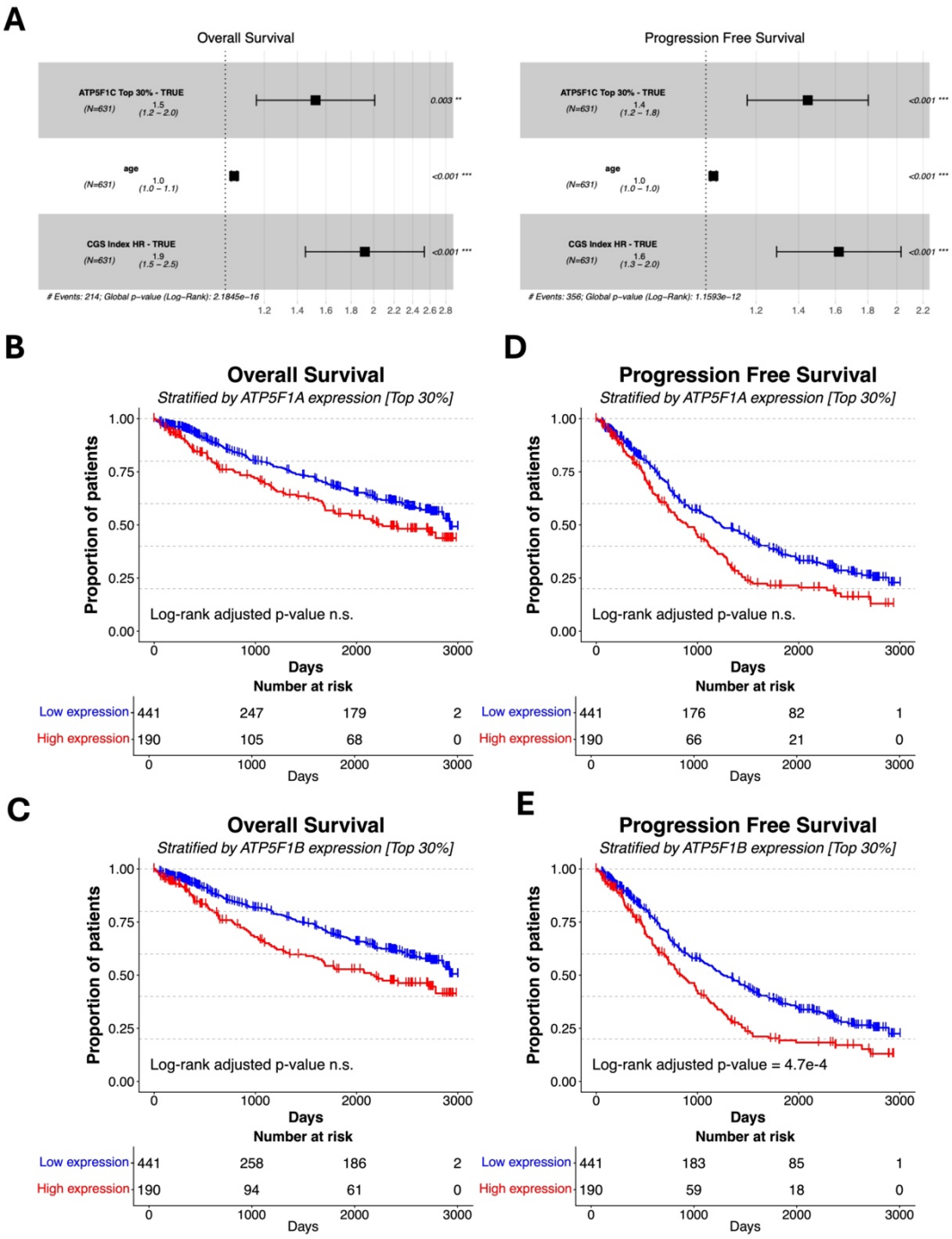

Supplementary Figure 12. Survival analyses and multivariable Cox regression models for ATP synthase subunits. (A) Multivariable Cox proportional hazards regression analysis showing the independent prognostic impact of ATP5F1C expression, age, and CGS high-risk classification on OS and PFS in MM patients from the CoMMpass study (IA21, n = 631). Hazard ratios (HR) with 95% confidence intervals are shown. ATP5F1C expression (top 30% vs remaining patients) and CGS status (high-risk vs standard-risk) were modeled as binary variables. Age was modeled as a continuous variable (per one-year increment). Statistical significance was assessed using the Wald test. **(B-E)** Kaplan–Meier survival curves for OS and PFS according to ATP5F1A and ATP5F1B expression levels in MM patients from IA21 CoMMpass study. Patients were stratified based on the top 30% of gene expression. Statistical significance was assessed using the log-rank test with correction for multiple testing (adjusted significance threshold $p < 0.001$).